Agricultural and Forest Meteorology 205 (2015) 83–95

Contents lists available at ScienceDirect

Agricultural and Forest Meteorology

journal homepage: www.elsevier.com/locate/agrformet

Understanding the variability in ground-based methods for retrieving canopy openness, gap fraction, and leaf area index in diverse forest systems

William Woodgate[a,b,*], Simon D. Jones[a,b], Lola Suarez[a,b], Michael J. Hill[c], John D. Armston[d,e], Phil Wilkes[a,b], Mariela Soto-Berelov[a,b], Andrew Haywood[b,e,f], Andrew Mellor[a,b,e,f]

[a] School of Mathematical and Geospatial Sciences, RMIT University, Melbourne, VIC 3001, Australia
[b] Cooperative Research Centre for Spatial Information, Carlton, VIC 3053, Australia
[c] University of North Dakota, Grand Forks, ND 58201, USA
[d] Department of Science, Information Technology, Innovation, and the Arts, Dutton Park, QLD 4102, Australia
[e] Joint Remote Sensing Research Program, School of Geography, Planning and Environmental Management, University of Queensland, St Lucia, QLD 4072, Australia
[f] Department of Environment and Primary Industries, East Melbourne, VIC 3002, Australia

ARTICLE INFO

Article history:
Received 20 October 2014
Received in revised form 17 February 2015
Accepted 18 February 2015

Keywords:
LAI
TLS
Hemispherical photography
Plant canopy analyser
Validation
Openness

ABSTRACT

Leaf area index (LAI) is a primary descriptor of vegetation structure, function, and condition. It is a vegetation product commonly derived from earth observation data. Independently obtained ground-based LAI estimates are vital for global satellite product validation. Acceptable uncertainties of these estimates are guided by satellite product accuracy thresholds stipulated by the World Meteorological Organisation (WMO) and the Global Climate Observing System (GCOS). This study compared canopy openness, gap fraction and LAI estimates derived from ground-based instruments; the primary focus was to compare high- and low-resolution (HR and LR) digital hemispherical photography (DHP) to a terrestrial laser scanner (TLS), augmented with measurements using the LAI-2200 plant canopy analyser in a subset of plots. Additionally, three common DHP classification methods were evaluated including a manual supervised (S) classification, a global (G) binary automated threshold, and a two-corner (TC) automated threshold applied to mixed pixels only. Coincident measurements were collected across five diverse forest systems in Eastern Australia with LAI values ranging from 0.5 to 5.5. Canopy openness, gap fraction and LAI were estimated following standard operational field data collection and data processing protocols. A total of 75 method-to-method pairwise comparisons were conducted, out of which 37 had an RMSD $\geq$ 0.5 LAI and 26 were significantly different ($p < 0.05$). HR-DHP (S) and two-corner (TC) methods were in close agreement with LAI-2200 (LAI RMSD 0.18 and 0.19, respectively). Additionally, the supervised (S) and two-corner (TC) methods were in close agreement over all canopy openness and LAI levels, matching to within 6% (openness: RMSD 0.04, LAI: RMSD 0.19). The automated classification method (TC) demonstrated the potential to be used as a substitute for the manual (S) classification (openness and LAI not significantly different, $p > 0.75$). Although TLS produced on average 55% higher openness and LAI than the HR-DHP (S) and (TC) classification methods, the strong coefficient of determination indicated the potential to calibrate these methods ($R^2 = 0.88$ and 0.79, respectively). Overall, results demonstrate a level of variability typically above the targeted uncertainty levels stipulated by the WMO and GCOS for satellite product validation. Further instrument calibration of TLS and improved DHP image capture and processing methods are expected to reduce these uncertainties.

1. Introduction

Leaf area index (LAI) is a primary descriptor of vegetation function and structure and an essential climate variable (GCOS, 2011). It is defined as one half of the total surface area of green leaves per unit

* Corresponding author at: Room 27, Level 11, Building 12, Remote Sensing Centre, School of Mathematical and Geospatial Sciences, RMIT University, Melbourne 3001, Australia. Tel.: +61 3 9925 2472.
E-mail address: william.woodgate@rmit.edu.au (W. Woodgate).

http://dx.doi.org/10.1016/j.agrformet.2015.02.012
0168-1923/

of ground area (Chen and Black, 1992). As leaf surface area of plant canopies is functionally related to the exchange of carbon dioxide, water and oxygen, total leaf area and its spatial distribution governs the energy and mass exchange by plant canopies between the lithosphere and atmosphere (Law et al., 2001; Spanner et al., 1990). LAI is directly related to the rate of canopy photosynthesis and evapotranspiration (Running, 1984; Running and Coughlan, 1988), and is therefore, a fundamental indicator of site water balance and rate of carbon sequestration (Gholz, 1982; Grier and Running, 1977). As a result, LAI is a key input parameter into a diverse range of application areas such as climate modelling, ecosystem productivity, weather prediction, agrometeorology, and hydrology (Garrigues et al., 2008a; Gobron, 1997; WMO, 2014). Monitoring LAI is essential for assessing the condition and development of vegetation worldwide (GTOS, 2009).

There are a range of global LAI satellite products such as the moderate resolution imaging spectroradiometer (MODIS) LAI (Knyazikhin et al., 1998), GLOBCARBON (Deng et al., 2006), and GEOV1 (Baret et al., 2013), which vary based on their spatial resolution, derivation method, and frequency of production (Camacho et al., 2013). Recent intercomparison and validation studies have highlighted LAI product uncertainties (Camacho et al., 2013; Fang et al., 2012). Fang et al. (2012) estimated MODIS collection 5 and CYCLOPES v3.1 (Baret et al., 2007) product uncertainty in the range of ± 1 LAI. Uncertainty for MODIS, CLYCLOPES, GLOBCARBON and GEOV1 satellite products evaluated by Camacho et al. (2013) ranged between 0.7 and 1.4 RMSE when compared with ground-based estimates (for LAI between 0 and 6). De Kauwe et al. (2011) found LAI product uncertainty was at its greatest (up to 36%) in areas of high LAI ($\approx$4 LAI in forests), and attributed this to saturation of the sensor signal used for the retrieval algorithm. Hill et al. (2006) found large LAI satellite product uncertainty in Australian forested environments partly attributing this to their predominantly erectophile leaf angle distribution (Anderson, 1981) and irregular tree and canopy architecture.

The value of satellite derived land surface products for decision making purposes is inextricably linked to the product's quality or accuracy (Cihlar et al., 1997). The Global Climate Observing System (GCOS) supported by the World Meteorological Organisation (WMO) have both specified target accuracy thresholds for global LAI products of 0.5 LAI units or a maximum of 20% LAI and 5% LAI, respectively. Cihlar et al. (1997) identified three methods for LAI validation: (i) comparing independently derived satellite products with one another, (ii) comparing outputs of physically based models describing the underlying processes governing the remote sensing signal, and (iii) comparing independent in-situ data to the product (this being the main approach). However, it is often implicitly assumed that in-situ data used for validation is 100% accurate (Cihlar et al., 1997).

In-situ estimates of LAI can be obtained using direct and indirect approaches, as described in comprehensive reviews by Bréda (2003), Jonckheere et al. (2004) and Zheng and Moskal (2009). In many in-situ protocols, (CEOS, 2014; ICOS, 2014; Schaefer et al., 2014; TERN, 2013), a range of instruments and measurement techniques are often specified, mainly focusing on indirect methods in forested environments due to their applicability over large areas and non-destructive nature. Each method has its own inherent biases and errors, which need to be better understood and quantified if the estimates are to be used for validation purposes (Camacho et al., 2013; Richardson et al., 2011).

Amongst the most common and mature indirect in-situ methods for estimating LAI, are digital hemispherical photography (DHP) and the LAI-2000 or 2200 plant canopy analyser (LI-COR Inc., NE, USA). More recently, terrestrial laser scanning (TLS) has provided an additional indirect ground-based technique to estimate LAI. TLS has also been used to derive a range of forest structure parameters including apparent canopy height profiles, stem density, and stem volume (Jupp et al., 2009; Lovell et al., 2003, 2011; Pueschel et al., 2013). These optical techniques estimate LAI through inversion of directional gap probability models using gap fraction data derived from the proportion of radiation intercepted by foliage elements in the canopy (Monsi and Saeki, 1965; Ross, 1981). Comparisons at the gap fraction level are essential for a better understanding of potential instrument differences (Leblanc et al., 2005). TLS has been proposed as a potential stable baseline estimate for gap fraction estimation due to its insensitivity to illumination conditions relative to passive remote sensing techniques (Danson et al., 2007; Seidel et al., 2012). This is in contrast to DHP gap fraction estimates, where variable sky illumination has been attributed as one of the main sources of error (Pueschel et al., 2012). Additional factors affecting direct comparison of in-situ instruments stem from instrument assumptions (Welles and Norman, 1991), multiple scattering of radiation affecting passive sensors (Kobayashi et al., 2013), instrument calibration (Danson et al., 2014; Lang et al., 2010), and application of different gap fraction and LAI retrieval methods and algorithms.

Over the past 25+ years, many studies have been undertaken to evaluate uncertainties with LAI estimation in forested environments, e.g. Chason et al. (1991); Coops et al. (2004); Macfarlane et al. (2007b); Whitford et al. (1995); Zhao et al. (2012). However, instrument-to-instrument comparison between these studies is limited by confounding influences of differing sampling designs, sample areas, and sensor field of view (Garrigues et al., 2008b). Furthermore, few studies have compared a TLS to DHP. Their conclusions with respect to the relative performance of TLS compared with DHP were limited by a number of factors. Such limiting factors included; different LAI retrieval algorithms applied to each instrument, comparing non-coincident LAI estimates from DHP to TLS (Lovell et al., 2003; Zhao et al., 2012); and comparing hemispherical photos to simulated hemispherical photos, based on multiple registered TLS scans at non-coincident locations to the real photos (Hancock et al., 2014; Seidel et al., 2012). These comparisons are not well suited for determining individual sensor differences.

Of the studies that conducted a direct comparison with hemispherical photography captured at the same measurement location as a TLS, either the key methodological step detailing camera exposure was not specified or automatic exposure was employed (Danson et al., 2007; Ramirez et al., 2013; Vaccari et al., 2012). Automatic exposure is known to greatly underestimate gap fraction in high LAI or forest environments due to image overexposure (Beckschäfer et al., 2013; Zhang et al., 2005). Additionally, comparison studies have typically chosen to employ only one DHP classification method. A number of classification methods are currently in use. These methods have the potential to be highly variable and have shown to have significant impact upon canopy openness, gap fraction and LAI estimates (Jonckheere et al., 2005; Macfarlane, 2011).

This paper presents, compares and contrasts the level of variance for estimating canopy openness, gap fraction, and LAI of four instruments following standard operational field data collection and data processing protocols (Leblanc et al., 2005; LI-COR, 2011). High- and low-resolution (HR and LR) digital hemispherical photography (DHP) are compared to a terrestrial laser scanner (TLS), augmented with measurements using the LAI-2200 plant canopy analyser in a subset of plots. Additionally, variances between three commonly used DHP classification methods are presented including; a supervised classification, a global automated threshold, and an automated classification method applied to mixed pixels after first identifying homogenous regions of canopy and sky. This paper makes recommendations regarding image classification procedure and discusses the utility for TLS to be used as a surrogate DHP or

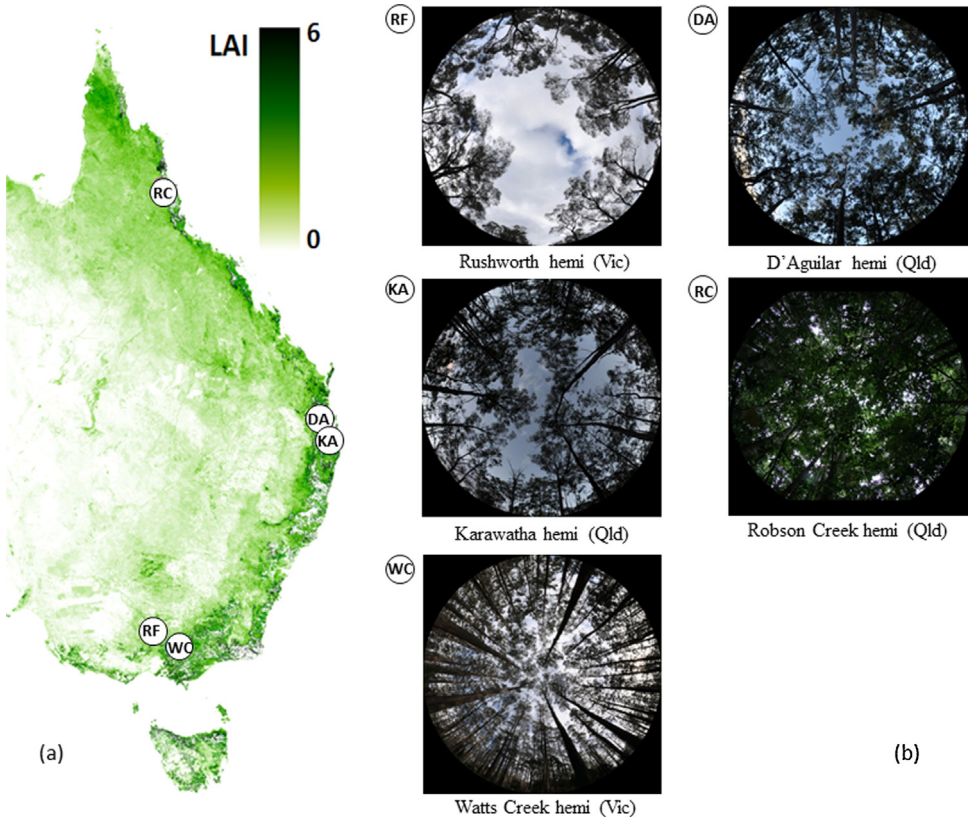

Fig. 1. (a) Location of study sites on the Australian east coast overlaid on MODIS LAI product (April, 2012), (b) representative hemispherical photos from each site; Vic (Victoria) and Qld (Queensland) denote the state.

LAI-2200 instrument for estimating openness, gap fraction, and LAI. Results over five representative forest types in Eastern Australia covering a range of LAI from 0.5 to 5.5 are presented.

2. Materials and methods

2.1. Study sites

Five study sites were selected covering a contrasting range of forest systems. The sites are all located along the east coast of Australia with LAI values ranging from 1 to 5 (Fig. 1). A brief summary of site characteristics including average LAI value, yearly rainfall and vegetation type is presented in (Table 1).

Rushworth (RF) is located in central Victoria. It comprises low open Box Ironbark forest with sparse understorey. The single-strata forest includes several eucalypt species such as Red Ironbark (*Eucalyptus sideroxylon*), Red Stringybark (*Eucalyptus macrorhyncha*), Red Box (*Eucalyptus polyanthemos*), Grey Box (*Eucalyptus microcarpa*) and associations with an average top of canopy height of 15 m.

Karawatha (KA) is located in southeast Queensland, south of Brisbane. The dominant vegetation types include a remnant dry sclerophyll eucalypt forest with a grassy understorey and remnant Melaleuca forest with a herbaceous understorey (Hero et al., 2013).

Watts Creek (WC) largely comprises a mature open forest of Mountain Ash (*Eucalyptus regnans*), which is amongst the tallest flowering plants, with some known to have reached heights in excess of 100 m (Ashton, 1976; Mifsud, 2003). Regrowth and older mature stands of Mountain Ash Shining Gum (*Eucalyptus nitens*) and Alpine Ash (*Eucalyptus delegatensis*) occur at higher elevations. Watts Creek is also characterised by dense understorey with patches of rainforest at lower elevations along the gullies.

D'Aguilar (DA) National Park is located in southeast Queensland, northwest of Brisbane. Woodlands and dry eucalypt forests mainly occur at lower elevations, whereas the forest becomes more complex at higher altitudes changing to wet sclerophyll or rainforest with thick understorey (Tree and Walter, 2012).

Robson Creek (RC) is located in Danbulla National Park within the Wet Tropics World Heritage Area of Far North Queensland. It consists of a mesophyll and notophyll vine forest and is floristically diverse. It has some of the highest biomass per hectare ratios found in the world (Bradford et al., 2014; Murphy et al., 2013). The canopy height ranges from around 25 m to 45 m.

Table 1
Site description of location, rainfall, dominant vegetation group and average MODIS LAI value.

Site	Location	Rainfall (mm/year)	NVIS vegetation group*	MODIS LAI^
Rushworth	36°45′S, 144°58′E	498	Eucalyptus open forests with a shrubby understorey	1.0
Karawatha	27°38′S, 153°05′E	909	Eucalypt open forest with a grassy understorey	1.4
Watts Creek	37°41′S, 145°41′E	1312	Eucalyptus tall open forest with a dense broad-leaved and/or tree-fern understorey	3.4
D'Aguilar	27°26′S, 152°50′E	1526	Eucalypt open forest with a grassy or shrubby understorey	4.7
Robson Creek	17°07 ′S, 145°38′E	2467	Warm temperate rainforest	4.8

*NVIS is the National Vegetation Information System classification (DEWR, 2007). Rainfall (mm/yr) represents the 30 year mean annual rainfall for that site with the exception of Karawatha and Robson Creek, estimated as the 12 year mean up to the year 2013. ^The MODIS LAI value refers to the study site's average LAI from the collection 5 MOD15A2 product since 2000.

Table 2
Summary of instrument characteristics used for the comparison.

Instrument	Model (manufacturer)	Angular resolution (degrees)	Maximum FOV (degrees) H, V	Wavelength (nm)
LAI-2200	LAI-2200 (LI-COR Inc.)	NA^^	300, 75**	<490
HR-DHP*	D90* (Nikon)	0.08	360, 90	400–700
LR-DHP	CI-110 (CID Inc.)	0.26	360, 92.5	400–700
TLS	VZ400 (Riegl)	0.06	360, 100^	1550

FOV is the field of view of the instrument in both horizontal (H) and vertical (V) directions, *denotes the Sigma EX 4.5 mm fisheye lens, was used with the HR DHP in all sites except Robson Creek where a Canon EOS 50D with a Sigma 8 mm fisheye lens was used, **denotes the FOV extent of the five discrete zenith rings of the LAI-2200, ^denotes the FOV of a single TLS scan. ^^The LAI-2200 outputs one value per sensor ring, therefore, the angular resolution is closest approximated by the bit-depth of the sensor (LI-COR, 2013; pers. comm., 16 April). The lens on the LR-DHP is a Sunex DSLR 215 with a prefabricated uniform neutral density filter and Infrared-cut coating. The maximum TLS measurement range for a natural target with 20% reflectivity is 160 m, with a 0.3 mrad beam divergence (Riegl, 2013).

2.2. Instruments

The specifications of the four instruments used in this study are described (Table 2). Data from each instrument is used to estimate the proportion of the field-of-view occupied by canopy gaps.

2.3. Data collection

Eleven plots were measured across the five study sites (Table 3) between March 2012 and August 2013. Plots were located well within natural stands of contiguous forest, each at least 100 hectares in size, thus, eliminating any sampling border effects from changing land systems. Not all instruments were used at each plot due to limited availability or inability to access a nearby open reference area for the LAI-2200. Therefore, LAI-2200 was used as a baseline comparison for LR- and HR-DHP methods in a subset of plots. To facilitate the comparison, each instrument was set-up using the same reference point on the ground at the same height (between 1 and 1.3 m above ground), with measurements taken only minutes apart. Coincident measurement locations were essential for subsequent comparison of instrument performance over the same field-of-view. Furthermore, measurements were taken in optimal diffuse lighting conditions for photography at dusk or dawn, or overcast diffuse conditions during the day. Wind was at most a minor presence in all acquisitions, and thus lead to few spurious returns and negligible blurring from moving canopy elements during scanning and photography acquisitions, respectively. Sampling design, i.e. the number and pattern of measurement locations, varied between some plots and sites. However, as the main objective was to compare instruments and their subsequent processing methods, the key methodological step of operating each instrument at the same point was deemed acceptable.

2.3.1. High-resolution digital hemispherical photography

The exposure and image selection technique used was based on Leblanc et al. (2005). In plot RF2 in Rushworth, an automatic exposure with fixed aperture was used, as it provided an optimally exposed image. In subsequent plots, multiple images were acquired at each point in JPEG fine format with camera bracketing set to ±1 f-stop, which changed the shutter speed automatically. The first image acquired was set to automatic exposure with exposure metering set to matrix metering. The set of images were then checked in the field using the image preview mode on the camera to ensure no over- or under-exposure. Image histograms were also previewed in the field using the camera's histogram function to check for a good separation of sky and canopy digital number peaks (Fig. 2). The selection criteria for the 'best' photo to process, was the photo that most clearly distinguished canopy elements from sky based on checks for over-exposure and under-exposure and good separation of histogram peaks. If none of the initial set of images fit the selection criteria, then the exposure level was stopped up or down accordingly by changing the shutter speed. This created redundancy in the image capture process. Photos were checked *a posteriori* in the lab to ensure the best choice from the field acquisition had been made. The camera was levelled using a triple axis level bubble fixed to the accessory shoe ensuring level to ±0.1°. Images were acquired pointing North.

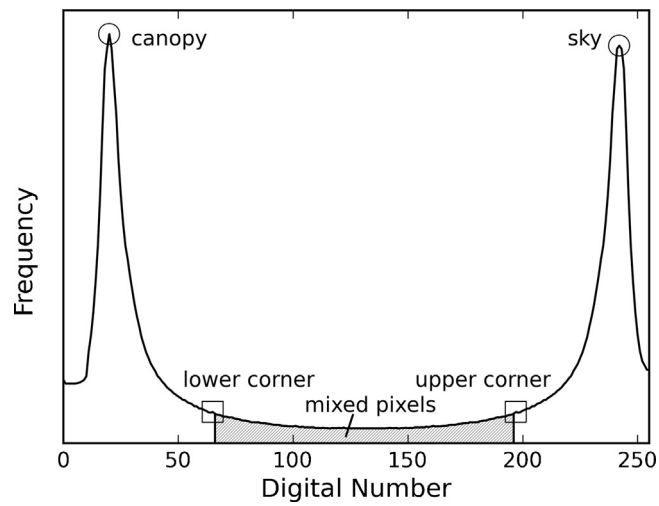

Fig. 2. An example of an ideally exposed image histogram. The histogram consists of two distinct sky and canopy peaks successfully identified by the two-corner classification method (Macfarlane, 2011); a large separation between sky and canopy peaks; minimal overexposure for sky pixels (pixels = 255 DN); minimal saturation of canopy pixels (DN = 0); and a small proportion of mixed pixels (shaded) between the lower and upper corner of the two-corner method. The proportions of sky and canopy pixels are approximately equivalent in the example.

2.3.2. Low-resolution digital hemispherical photography

Images were captured using LR-DHP in 'preview' mode following an adapted protocol of Leblanc et al. (2005). The LR-DHP instrument did not provide a function to conduct a visual inspection of the histogram in the field. Therefore, only the image preview mode of the instrument was used as a guide when modifying

Table 3
Plot description with instruments used, number of sample points, and plot dimensions.

Plot name*	Instruments	Sample points	Plot dimensions
RF1	TLS, HR-DHP	4	30 m radius
RF2	LAI-2200, HR- & LR-DHP	72	25 m x 25 m
RF3	LAI-2200, HR- & LR-DHP	6	25 m x 25 m
RF4	TLS, HR-DHP	5	40 m radius
KA1	TLS, HR-DHP	5	50 m x 50 m
KA2	TLS, HR-DHP	5	50 m x 50 m
DA1	TLS, HR-DHP	5	50 m x 50 m
WC1	LAI-2200, HR- & LR-DHP	11	50 m transect
WC2	HR- & LR-DHP	11	100 m transect
RC1	TLS, HR- & LR-DHP	5	50 m x 50 m
RC2	HR- & LR-DHP	5	30 m x 30 m

*RF: Rushworth, KA: Karawatha, DA: D'Aguilar, WC: Watts Creek, RC: Robson Creek.

camera settings to determine an optimally exposed image. The aperture of the instrument is fixed at a manufacturer specified value of f 2.8. Images were acquired pointing North. The camera was levelled using a self-levelling gimbal mount fixed to a hand-held wand. High quality conversion of PNG to JPEG formats was conducted in IrfanView v4.36 (Skiljan, 2013). Based on visual and histogram inspection of the digital number frequencies, there were no compression/conversion artefacts from the PNG lossless image format to the JPEG format.

2.3.3. Terrestrial laser scanner

At each measurement location, the TLS scanned the hemisphere in two parts. First a horizontal scan from 30 to 130° zenith was acquired, then the instrument was tilted at 90° and the upper hemisphere was scanned. For the analysis, the 0–30° section was used from the tilted scan and greater than 30° zenith angle was used from the horizontal scan. The horizontal and tilted scans were registered to within 1 cm precision using common retro-reflective targets in the field and RiSCAN software (Riegl, 2010). The angular resolution was set at 0.06° for all scans at every plot. More technical information on the Riegl VZ400 can be found in (Riegl, 2013). Lighting conditions have a negligible impact on the TLS as its wavelength is 1550 nm and it is an active emitter of radiation.

2.3.4. LAI-2200

The LAI-2200 was operated in dual-wand mode with a synchronised and levelled reference sensor operating autonomously located in a nearby open area (<2 km), consistent with best practise guidelines as outlined in the manufacturer manual (LI-COR, 2011). The sky conditions were partially cloudy at the times of dawn or dusk when the LAI-2200 was operated, with slow moving clouds that lead to a stable lighting environment for both reference and measurement sensors. A 90° view cap was placed on both sensors to mask the operator. The orientation of the cap was recorded with a compass to maintain consistency with plot measurements. The LAI-2200 is designed to produce the same results as its predecessor, the LAI-2000.

2.4. Data processing and analysis

2.4.1. Digital hemispherical photography

Hemispherical photos were classified in a number of standard ways. The first method was a supervised classification conducted the CanEye software (Weiss and Baret, 2014). Two automated image classification approaches were also applied: a global binary threshold using the Ridler and Calvard (1978) method; and a two-corner method from Macfarlane (2011) to first classify homogenous regions of sky and canopy. Three classification techniques were then applied to the mixed pixels. Camera lens projection functions and image-lens image centre offset calibrations were applied for all photography. All images were masked to a 150° field of view, coinciding with the lowest zenith angle of the LAI-2200. Restricting the FOV minimises the increased frequency of mixed pixels at low zenith angles and ensures background pixels of circular fisheye images do not bias automated classification algorithms operating at the image histogram level.

2.4.1.1. Supervised classification (S). The same experienced operator was used for the supervised classification to reduce operator bias caused by subjectivity (Beaudet and Messier, 2002). Images were processed in CanEye v6.3.11, with no gamma correction. Pixels were classified into a binary image of sky or non-sky. Image resolution was preserved (i.e. no pixel subsampling), however, a default k-means clustering colour palette reduction takes place in CanEye based on minimum variance quantization (rgb2ind MATLAB function; Mathworks Inc., MA, USA) resulting in a reduction of the number of colours to 324 to aid in the supervised classification process (Weiss and Baret, 2014; Weiss, 2014 pers. comm., 15 October). This colour reduction was conducted in addition to the initial in-camera JPEG compression. The magnitude of the effect of the additional colour reduction on the classification of the image is unknown.

2.4.1.2. Automated thresholds (AT). Automated threshold techniques provide an objective comparison removing the operator bias which is known to be large (Jonckheere et al., 2005). The blue channel of the in-camera image was used for both HR- & LR-DHP cameras as it is known to be least affected by multiple scattering of radiation under the canopy (Welles, 1990). Furthermore, the blue channel presents the highest contrast between the foliage and sky, which allows for better separation into two classes (Jonckheere et al., 2005). Background pixels were masked (i.e. those pixels outside the projected image of canopy) to avoid bias in the threshold computation.

The first AT method applied to the imagery was the global binary automated threshold method from Ridler and Calvard (1978), referred to as global (G). The iterative clustering technique calculates a global threshold based on the clustering of image intensity levels of the blue channel. In 2005, Jonkheere et al. found Ridler and Calvard's (G) threshold to be the most robust method for a wide range of light and canopy structure conditions.

The second AT method applied was the two-corner classification procedure, referred to as two-corner (TC), from Macfarlane (2011) using the DCP toolbox version 3.14 (Macfarlane et al., 2014). The automated procedure first identifies the unambiguous sky and canopy peaks of the image histogram, and then detects the digital numbers 'DN' at the point of maximum curvature to the right of the canopy peak, and to the left of the sky peak, i.e. the lower (DNl) and upper (DNu) corners (Fig. 2). Mixed pixels containing a portion of canopy and sky, located between the lower and upper corners of the image histogram (Fig. 2), were classified with the dual binary threshold (Macfarlane, 2011; Macfarlane et al., 2014). The dual binary threshold first identifies gaps smaller than 1% of the image size in the regions previously classified as canopy and applies the threshold $DN = [DNl + (DNu - DNl) \times 0.25]$ to minimize the loss of small gaps. In the remainder of the image, a higher threshold ($DN = [DNl + (DNu - DNl) \times 0.75]$) was applied to the mixed pixels to minimize the loss of canopy elements located in bright regions of the image. The end result is a binary image of sky or canopy pixels. A comparison of results of the dual binary classification with other in-built classification procedures in the DCP toolbox yielded similar results due to low proportions of mixed pixels in the DHP imagery, typically between 2% and 15%. Therefore, for conciseness of results only the dual binary threshold method was presented.

Automated thresholds were not applied to LR-DHP images due to the algorithm's inability to distinguish homogenous regions of canopy and sky in a majority of images. This was caused by low dynamic ranges between sky and canopy pixels. Although care was taken to minimise overexposure, the result was a poorer separation of sky and canopy in the image histogram. This was only identified in a post-processing stage due to no image histogram preview function offered by the LR-DHP camera. HR-DHP was not affected to the same degree as LR-DHP, although HR-DHP also exhibited some dual peaks of sky and canopy under these conditions. Thirteen of the total 134HR-DHP images failed to automatically correctly classify homogenous areas of sky and canopy. This was primarily caused by dual peaks of canopy, sky, or a combination of both. In these cases, a manual threshold was applied based on the image histogram.

2.4.2. Canopy openness and gap fraction

Canopy openness was calculated for HR- & LR-DHP images as the proportion of sky pixels to total pixels in the 150° field-of-view

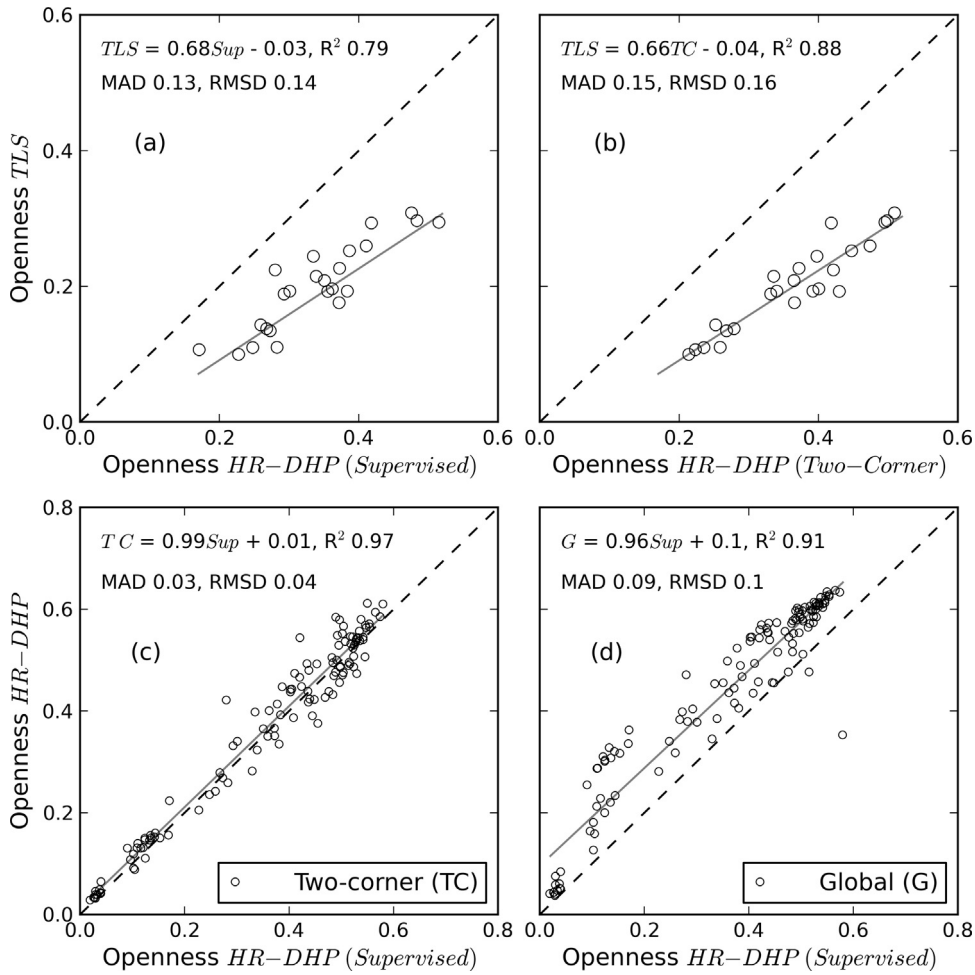

Fig. 3. Canopy openness of the HR-DHP supervised classification (a) and two-corner (TC) classification (b) versus TLS openness for all concurrent plots (RF1, RF4, KA1, KA2, and DA1). Canopy openness of the HR-DHP supervised (S) method versus; openness from the two-corner (TC) classification method (c), and openness from the global (G) classification method using the Ridler and Calvard (1978) algorithm (d) for all plots. Non-fitted reduced major axis linear regression line (grey) and equation (inset) shown, $p < 0.01$. Mean absolute difference (MAD) and root mean square deviation (RMSD) provided inset. The 1:1 line is dashed.

(FOV). TLS openness was calculated from the proportion of outgoing pulses that did not record a return over the same FOV. Gap fraction of the classified hemispherical photos was derived from the proportion of sky pixels as a function of zenith view angle. Gap fraction from the LAI-2200 was estimated from the intensity of light measured under the canopy divided by the reference sensor readings for the five instrument zenith rings. Gap fraction from the TLS was estimated from the number of outgoing pulses returned as a 'hit' divided by the total number of outgoing pulses as a function of zenith angle, also known as a point-based method (Danson et al., 2007). Gap fraction from the TLS and DHP instruments were convolved into 2.5° zenith bins to reduce minor levelling and geolocation errors. For plots, where the LAI-2200 was operated, gap fraction was convolved into the five discrete zenith rings of the LAI-2200 for direct comparison at the gap fraction level.

2.4.3. Effective LAI

LAI was calculated using a modified version of Miller's LAI formula (Eq. (1)) (LI-COR, 2011; Miller, 1967; Welles and Norman, 1991). (Eq. (1)) integrates gap fraction over a range of zenith angles. For each zenith annuli, foliage density is calculated and then a weighting function (Eq. (2)) is applied correcting for the path length through the canopy. The formula assumes the canopy is horizontally homogenous (LI-COR, 2011). Miller's formula provides a measure of effective LAI (LAIe), i.e. no foliage clumping correction. The product of the clumping correction factor and LAI provides LAIe (Chen and Black, 1992).

$$\mathrm{LAIe} = 2\int_0^{\pi/2} -\ln(P_o(\theta_v))\cos\theta_v \sin\theta_v d\theta_v \quad (1)$$

where P_o denotes the gap fraction and θ_v denotes the view zenith angle. P_o is averaged per zenith segment or 'ring' for input into (Eq. (1)). Utilising zenith rings allows discretisation of the instrument field-of-view into smaller zenith segments in order to compute multiple P_o estimates for input into (Eq. (1)). The application of Eq. (1) using multiple angular, P_o estimates for each measurement location is weighted using (Eq. (2)).

$$W_i = \frac{d\theta_i \times \sin\theta_i}{\Sigma_{i=1}^{i=n} d\theta_i \times \sin\theta_i} \quad (2)$$

where i is the zenith ring number, n is the number of zenith rings, θ_i is the ring centre angle, and $d\theta_i$ is the angular ring width. The sum of W_i, the zenith ring weighting function (Eq. (2)), for all n is equal to unity. Gap fraction from each instrument was convolved into the five discrete zenith rings of the LAI-2200, i.e. zenith rings centred at 7°, 23°, 38°, 53°, and 68° zenith angles, (LI-COR, 2011). This ensured that the same angular zenith range was used for each method for comparison. Individual measurement LAI was subsequently computed for each instrument using the first four equivalent LAI-2200 zenith rings. The equivalent fifth zenith ring of the LAI-2200 was

not used to minimise the effect of increased mixed pixels at low zenith angles (Jonckheere et al., 2004; Leblanc et al., 2005). Plot effective LAI was calculated for each method utilising gap fraction from the first four equivalent LAI-2200 zenith rings. It was calculated by first averaging gap fraction for the plot for each zenith ring, and then applying (Eq. (1)). By first averaging the individual measurement gap fractions comprising a plot and then applying (Eq. (1)), instead of averaging individual effective LAI values comprising a plot, a correction for non-random canopy elements is avoided from the potential logarithmic averaging of LAI that may occur at multiple measurement locations (Kucharik et al., 1997; Ryu et al., 2010).

LAI from (Eq. (1)) enabled direct comparison of instruments because; (i) gap fraction from the same portion of the hemisphere of each instrument at each concurrent measurement location was used, and (ii) applying different LAI algorithms to different instruments may bias or confound results. Alternative methods to estimate LAI were not included in this study as they depart from comparison at the gap fraction level or they employ different equations prohibiting a direct comparison of the instruments. As no distinction was made between foliage and non-foliage elements such as trunks and branches, the metric derived was plant area index (Chen et al., 1991). A site specific woody-to-total plant area, correction factor was not applied nor derived in this study, as it would be constant for all methods, thus, not enhancing method-to-method comparisons. Therefore, the metric will be referred to as LAI from here onward for consistency.

2.5. Data and method comparison

Linear non-fitted reduced major axis (RMA) regression analysis was used to compare retrieval methods of openness and LAI. RMA regression is specifically formulated to handle errors in both the x and y variables. Therefore, it is suitable for pairwise method comparisons in this study as all methods are treated as independent variables due to the absence of a direct 'truth', which is not feasible to obtain from destructive harvesting in forests. The offset and slope of the RMA regression equation revealed the degree of any systematic differences between methods; and the coefficient of determination (R^2) provided a measure of the strength of the relationship. Two-way analysis of variance (ANOVA) was conducted on openness and LAI to detect significant differences between retrieval methods and plots. If the ANOVA revealed significant differences, Tukey's honest significance difference (HSD) test was conducted post-hoc to determine which combination of methods and plots had significant differences ($p < 0.05$). Plot average method gap fraction and LAI were graphed to provide a visual representation of canopy structure and method variability. Lastly, root mean square deviation (RMSD) and Mean absolute deviation (MAD) were estimated for measurement pairs to determine the level of openness and LAI variance. Statistical analysis was conducted in IBM SPSS statistics v22 (IBM Corp.).

3. Results

3.1. Openness

Although the canopy openness from TLS was significantly different to the HR-DHP supervised (S) and two-corner (TC) classifications (ANOVA, $p < 0.05$), a strong correlation between the methods was observed (Fig. 3a and b). The interaction term between these methods and plots was not significant (ANOVA, $p > 0.36$). The only plot where the (S) method openness was not significantly different to TLS was in KA2, due to more closely matching gap fractions compared with other plots (Fig. 4), coefficients of

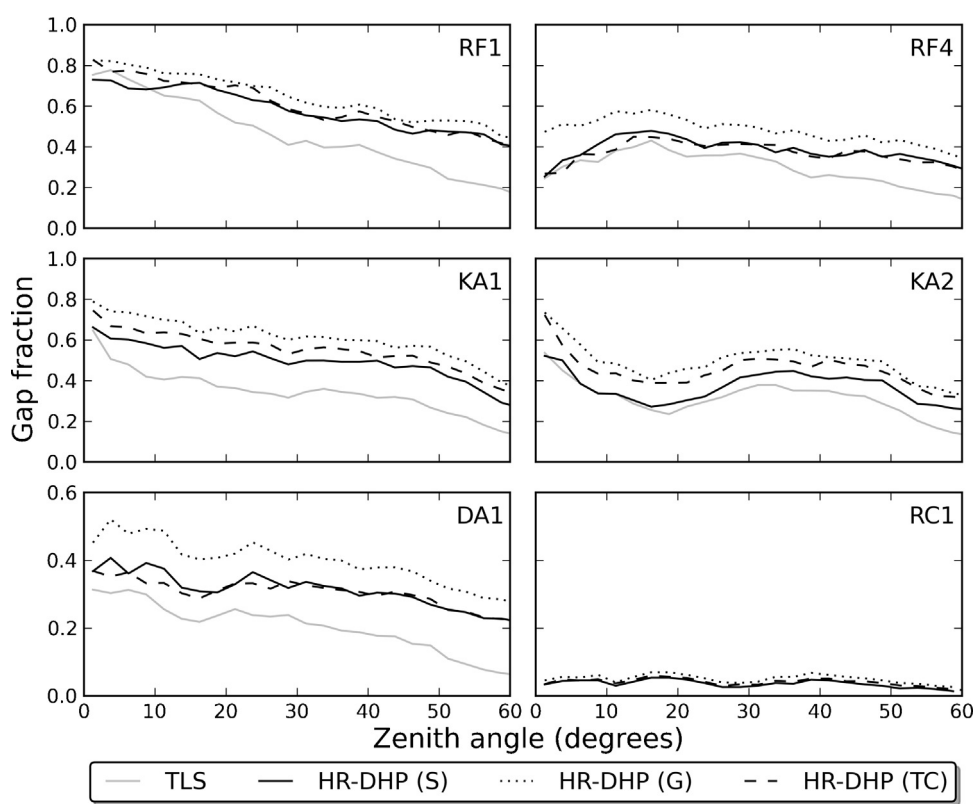

Fig. 4. Average plot gap fraction in 2.5° zenith bins versus zenith angle for the six TLS plots; TLS (solid grey line), HR-DHP supervised classification (HR-DHP (S), solid black line), HR-DHP global binary classification using the Ridler and Calvard (1978) algorithm (HR-DHP (G), dotted black line), and HR-DHP two-corner method using the dual binary classification (HR-DHP (TC), dashed black line).

determination (R^2) for the (S) and (TC) classifications with TLS were 0.79 and 0.88, respectively. The intercept and slope of the reduced major axis linear (RMA) regression function matched very closely for both HR-DHP methods with TLS, with the higher correlation achieved by the (TC) classification method. RC1 results were not presented due to no-data, TLS returns caused by the close proximity of foliage to the scanner (<1.5 m). This did not occur at any other plots.

A strong linear correlation ($R^2 = 0.97$) was observed between the two-corner (TC) method and the supervised (S) classification of HR-DHP with no bias (intercept almost 0, $p < 0.01$, Fig. 3c and d). The ANOVA revealed no significant difference between the two methods ($p > 0.58$). The intercept and slope of the linear RMA regression function between (S) and (TC) methods were not significantly different to zero and one, respectively. Contrastingly, a large 0.1 offset ($p < 0.01$) between HR-DHP (S) and the global (G) openness was found, in addition to significantly different openness values ($p < 0.01$). This disparity was further highlighted by the smaller RMSD and MAD for HR-DHP (S) with (TC) (0.03 for both) as opposed to the HR-DHP (S) with (G) method (0.1 and 0.09, respectively). For HR-DHP (S) with (G), generally as openness increased, the proportional difference between the supervised and global classifications decreased. For example, at 10% openness for the (S) method, the openness for the (G) method ranged between 10% and 30%; whereas at 50% openness for the (S) method, the openness for the (G) method ranged between 50% and 60%. Thus, the proportional difference was less for higher openness, indicating lower variability of the (G) classification method with higher openness levels.

The (G) threshold for all 134HR-DHP images was within the sky and canopy peak DN range as identified by the (TC) method. Ten of the 134 (G) images produced thresholds outside the lower and upper corner DN values, 9 of which were less than the lower corner. Additionally, the (G) threshold was consistently lower (72% of images) than the mid-point between the lower and upper corners, thus, leading to a threshold comparatively favouring the classification of sky over foliage.

3.2. Gap fraction

Fig. 4 reveals the presence/absence of dominant gaps and canopy structure due to the narrow bin sizes (2.5°). Plot average gap fraction estimates showed the general characteristic decay with increasing zenith angle for each method, due to longer path lengths at higher zenith angles (Figs. 4 and 5). However, plot KA2 exhibited a spline gap fraction caused by increased gaps near zenith and 30–40° zenith angles relative to 10–30° and >40° zenith angles. Additionally, plots RF4 and RC2 gap fraction at zenith were lower than at larger zenith angles (>40°), caused by the relative lower gap proportion. This is not uncommon for plots where only 4–5 measurements are averaged. Determining a representative estimate of gap fraction near a view angle of 0° may require a large number of measurements (>20) due to comparatively smaller sampling areas (Macfarlane et al., 2007a).

A closely matching gap fraction (±0.1) near zenith was observed for TLS and HR-DHP (S) in all plots (Fig. 4). The HR-DHP (TC) and (G) classifications were typically within 5% gap fraction over all zenith angles. HR-DHP (G) gap fraction was the highest for all plots over all zenith angles (Fig. 4). An observed trend was TLS gap fraction typically decreased with zenith angle at a higher rate comparatively to all HR-DHP classifications. Subsequently, TLS displayed the lowest gap fraction at the largest zenith angle. The magnitude of the TLS gap fraction offset to the HR-DHP methods at the 60° zenith angle was between 0.15 and 0.2, where the HR-DHP methods matched to within 0.1 gap fraction. The lower TLS gap fraction was also evident in canopy openness (Fig. 3a and b).

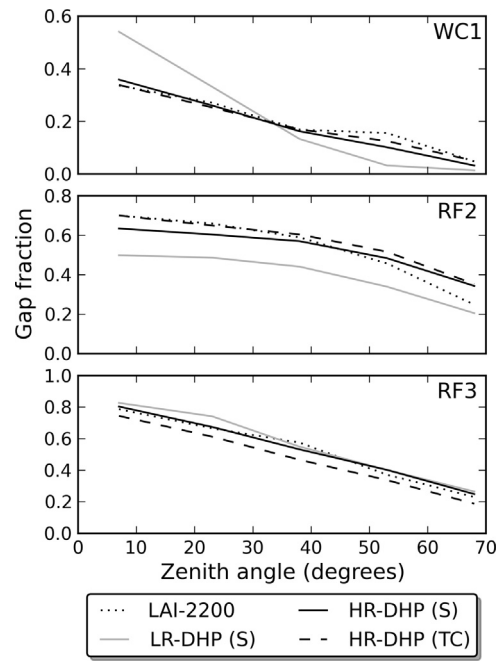

Fig. 5. Average plot gap fraction aggregated to the five zenith rings of the LAI-2200 versus zenith angle for the three plots where the LAI-2200 was operated. Methods shown consist; LAI-2200 (dotted line), low resolution-DHP supervised (LR-DHP (S), solid grey line), high resolution-DHP supervised (HR-DHP (S), solid black like), and high resolution-DHP two-corner (HR-DHP (TC), dashed line).

A relatively smooth gap fraction profile was observed in Fig. 5 due to aggregation of gap fraction into larger zenith bins (≈10° versus 2.5° in Fig. 4). HR-DHP (S) and (TC) typically matched within 0.1 gap fraction of the LAI-2200. The next closest to method to HR-DHP (S) was HR-DHP (G). However, HR-DHP (G) displayed on all occasions the highest gap fraction of all HR-DHP and TLS methods (Figs. 4 and 5). Gap fraction from the LR-DHP (S) method was the furthest off the LAI-2200 in RF2 and WC1; up to 0.25 gap fraction and typically greater than 0.1–0.15 for most zenith angles (Fig. 5).

3.3. LAI

The plot mean LAI values for each method demonstrated that all methods revealed ecotonal changes present between sites (Fig. 6). The LAI values for the sites ranged from 0.5 to 5.5 across all retrieval methods. The estimated LAI values for each plot would be expected to be higher, once foliage clumping effects were taken into account (Chen and Black, 1991). Within-plot variability of LAI(plots RF1-4, KA1-2, DA1, WC1-2, RC1-2), represented by the 1 standard deviation extent in Fig. 6, demonstrates the level of plot heterogeneity as estimated by the various retrieval methods.

On average, HR-DHP (S) was within 6% LAI of HR-DHP (TC) for all plots, and not significantly different at any plot (Tukey HSD, $p > 0.9$). In addition, the HR-DHP (TC) and (S) methods were within 9% LAI of LAI-2200 (RMSD 0.18 and 0.19 LAI, respectively), and were not significantly different at any plot ($p > 0.75$). On the other hand, HR-DHP (S) and (TC) were on average 34% and 29% LAI higher than (G), with significant differences in 4 plots (RF2, WC1-2, RC1) and 3 plots (same plots without RC1), respectively (Fig. 6, Table 4). All HR-DHP classification method comparisons revealed LAI differences that were not correlated with plot LAI ($R^2 \approx 0$); using HR-DHP (S) for the plot LAI level.

At each plot, the within-plot LAI variance, as demonstrated by the ±1 standard deviation error bars in Fig. 6, was approximately

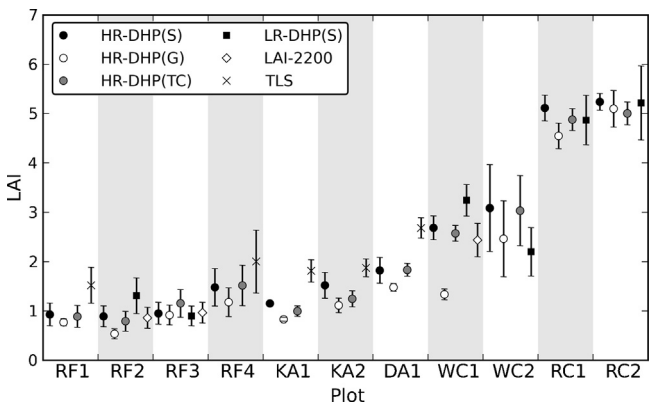

Fig. 6. Mean LAI plot values for each method at all sites. The errors bars denote ±1 standard deviation of individual plot LAI measurements. Plot abbreviations: Rushworth (RF), Karawatha (KA), D'Aguilar (DA), Watts Creek (WC), Robson Creek (RC). Instrument abbreviations: high/low resolution (HR/LR) digital hemispherical photography (DHP). Classification method abbreviations for DHP: supervised (S), global (G), and two-corner (TC).

equivalent for all methods with the exception of TLS and HR-DHP (G). In other words, the HR-DHP (S), (TC) and LR-DHP (S) methods were producing similar plot level LAI variance, whereas the TLS and HR-DHP (S) methods were producing comparatively higher or lower levels of within-plot variance, respectively. HR-DHP (G) produced an equivalent or smaller plot LAI variability to all other methods in the TLS plots, exhibiting the smallest coefficient of variation 'CV' (average CV = 0.11 compared with 0.18, 0.16, and 0.17 for HR-DHP (S), (TC), and TLS, respectively). In plots RF1-2, KA2, DA1, and WC1, the HR-DHP (G) method demonstrated a comparative insensitivity to within-plot LAI variability as found with other methods.

TLS produced the highest plot LAI values compared to all HR-DHP methods in all five plots (Fig. 6). On average, TLS was 90%, 55%, and 50% LAI greater than HR-DHP (G), (TC) and (S) methods, respectively. TLS was significantly different (Tukey HSD test, $p < 0.05$) from: HR-DHP (S), (G) and (TC) in plots KA1 and DA1; HR-DHP (S) and (G) in plot KA2; and HR-DHP (G) in plot RF4. Interestingly, in plot KA2 the LAI was significantly different for the (S) method with TLS, which was in contrast to canopy openness. This can be explained by the larger deviations in gap fraction between the two methods occurring at lower zenith angles (Fig. 4), where the LAI formula implemented is weighted more heavily (Eqs. (1) and (2)). The comparatively larger LAI estimates from TLS was evident from the steeper slope and intercept of the reduced major axis linear regression functions fitted with TLS and all other methods (Table 4). The large TLS offset was substantial (>0.5 or 20% LAI in all cases).

HR-DHP (G) consistently produced one of the lowest plot average LAI estimates (9 of 11 plots) of all methods. On average (G) was 27% LAI less than LAI-2200. The large LAIdifferences and steep slope (slope = 1.66 × LAI-2200) for the HR-DHP (G) and LAI-2200 RMA function in Table 4 was primarily due to very low HR-DHP (G) LAI values in plot RF2 and WC1 (both plots significantly different, $p < 0.05$). On the other hand, LR-DHP (S) was on average 30% LAI higher than LAI-2200 and significantly different at the same two plots as HR-DHP (G).

Reasonably high coefficients of determination values ($R^2 > 0.7$) were obtained for all comparisons (Table 4). RMSD LAI estimates for the 13 possible method combinations ranged from 0.18 to 1.07. Eight of those method combinations had an RMSD greater than 0.5 LAI; the majority involved TLS or LR-DHP (S). In every plot where LAI-2200 was operated, it matched closest with HR-DHP (S) and (TC) gap fraction and LAI (no significant differences), with an RMSD of 0.19 and 0.18, respectively (Table 4).

4. Discussion

In this study, a total of 75 indirect method-to-method pairwise comparisons were conducted across 11 plots (sum of top diagonal of Table 4). Out of 75 comparisons, 37 had an RMSD ≥ 0.5 LAI and 26 were significantly different (Tukey HSD, $p < 0.05$). For sites with low LAI, 0.5 represents a large proportion of the total leaf area index. A key point is that LAI accuracy targets for satellite products specified by GCOS and the WMO are for the satellite products estimates to match within 0.5 LAI or as low as 5% of ground-based estimates. Independently obtained ground-based estimates require a much smaller degree of relative uncertainty to one-another than generally found in this study in order to be used with a high degree of confidence.

The LAI-2200 and its predecessor the LAI-2000 have been used as a benchmark instrument for gap fraction and LAI estimation (Lang et al., 2010; Pueschel et al., 2012). In a subset of plots, the two methods presenting the best agreement with the LAI-2200 were the HR-DHP supervised (S) and two-corner (TC) classifications, with the lowest RMSD LAI values and no significant differences. LAI-2200 plot average LAI matched to within 10% for both of those methods (RMSD 0.19 and 0.18 LAI, respectively). The close degree of matching is encouraging considering Welles and Norman (1991) found

Table 4
Method-to-method comparison table.

		HR-DHP (S)	HR-DHP (G)	HR-DHP (TC)	LR-DHP (S)	LAI-2200	TLS	
HR-DHP (S)	$y = ax + b$	x	11, 4 (134)	11, 0 (134)	6, 2 (99)	3, 0 (89)	6, 3 (29)	Plots, Sig. (points)
	R^2	1	0.60	0.21	0.58	0.19	0.74	RMSD
HR-DHP (G)	$y = ax + b$	$0.84x - 0.23$	x	11, 3 (134)	6, 3 (99)	3, 2 (89)	6, 3 (29)	Plots, Sig. (points)
	R^2	0.94	1	0.50	1.07	0.52	1.07	RMSD
HR-DHP (TC)	$y = ax + b$	$0.93x + 0.02$	$1.05x + 0.33$	x	6, 2 (99)	3, 0 (89)	6, 2 (29)	Plots, Sig. (points)
	R^2	0.98	0.95	1	0.63	0.18	0.75	RMSD
LR-DHP (S)	$y = ax + b$	$0.92x + 0.55$	$0.97x + 0.94$	$0.97x + 0.53$	x	3, 2 (89)	0	Plots, Sig. (points)
	R^2	0.92	0.82	0.92	1	0.61		RMSD
LAI-2200	$y = ax + b$	$0.89x + 0.06$	$1.66x - 0.04$	$0.91x + 0.09$	$0.72x - 0.08$	x	0	Plots
	R^2	0.92	0.82	0.91	0.84	1		
TLS	$y = ax + b$	$1.16x + 0.49$	$1.77x + 0.2$	$1.18x + 0.49$	NA	NA	x	
	R^2	0.79	0.69	0.88			1	

Bottom diagonal: reduced major axis (RMA) regression equations for all individual LAI measurements with the coefficient of determination (R^2); columns headers as the independent variable (x), row headers as the dependent variable (y). Top diagonal (shaded): the number of plots comparing the methods, the number of significantly different plots 'Sig. ' (Tukey HSD, $p < 0.05$), and total number of measurement locations in brackets; below is the Root mean square deviation (RMSD, LAI unitless). The automated classifications (G and TC) for LR-DHP were not included due unsuitable image histograms.

repeated LAI-2000 measurement error up to 15% LAI. The cause of bias between LAI-2000 and DHP methods has been previously attributed to calibration errors or differences in sky illumination, leading to random errors of 5% and 10% in LAI, respectively (Richardson et al., 2011). Additional factors influencing the direct comparison of these instruments include minor instrument levelling errors from handheld instruments (Lang et al., 2010), the 90° view cap masking out the operator, and potential multiple scattering effects leading to an overestimation of gap fraction (Kobayashi et al., 2013). However, this study compared further factors such as two different resolution hemispherical cameras and three different classification methods; one supervised and two automated classifications.

Automated threshold classifications negate operator induced biases and inconsistencies typically found in manual supervised approaches (Jonckheere et al., 2005). The two automated approaches applied to the HR-DHP imagery differed substantially from one another (RMSD 0.5 LAI), and were significantly different in three plots ($p < 0.05$; RF1, WC1-2). The (G) method presented the highest openness and gap fraction (Figs. 3 and 4) and lower LAI (Fig. 6). The (G) classification method was less sensitive to within-plot LAI ranges compared with the other methods as denoted by the ±1 SD bars in Fig. 6. Additionally, the (G) method produced higher RMSD when compared with (TC), using the LAI-2200 as a basis for comparison (RMSD 0.52–0.18 LAI, respectively; significantly different, $p < 0.05$). Lastly, the closer agreement of (S) with LAI-2200, (S) with (TC), and (TC) with LAI-2200 over (G) (lower RMSD and fewer significantly different plots; Table 4) indicated that the (TC) classification method provided a better agreement of openness, gap fraction and LAI estimates with (S) and the LAI-2200 over the global classification method (G).

The main difference between the automated two-corner (TC) and global (G) approach was the (TC) threshold was applied to only the mixed pixels identified from first classifying the image into homogenous regions of canopy and sky (Macfarlane, 2011). Advantages of applying a classification algorithm to only the mixed image pixels are the reduced likelihood of gross classification errors, and low gap fraction sensitivity from the classification algorithm due to mixed pixels typically accounting for less than 10% of the image (Macfarlane, 2011; Macfarlane et al., 2014; this study). Although in dense forest environments, a small gap fraction deviation may lead to a large LAI difference due to the exponential relationship of gap fraction to LAI (Eq. (1)). A remaining limitation of matching DHP gap fraction estimates with a reference or benchmark gap fraction becomes the determination of optimal camera exposure, which will be discussed further.

A fundamental difference between the DHP and LAI-2200 methods is the need for determining optimal exposure and subsequent classification of DHP images as opposed to LAI-2200. The LAI-2200 avoids the need for determining exposure as it has 16-bit precision measured over four decade ranges of logarithmic scale (e.g. 1/10, 1/100, and 1/1000) enabling sensitivity from very low light levels through to direct measurement of sunlight (LI-COR 2013, pers. comm., 16 April). However, this advantage is partially offset with the difficulties of finding an open reference area which may not be feasible in many forested areas, and potential errors introduced from partially cloudy or uneven sky conditions in the plot location and reference area.

Image exposure, processing and subsequent classification procedures have been identified as the major error components for DHP gap fraction estimation (Beckschäfer et al., 2013; Pueschel et al., 2012; Rich, 1990). This study utilised 'optimally' exposed in-camera JPG images, selected based on the image histogram and image preview. The general range of optimal exposure for this study was between automatic exposure (AE) and 2 stops under AE. In-camera, JPG images have limited radiometric resolution (8 bit), making image classification sensitive to image exposure (Macfarlane, 2011). Authors have suggested techniques to counter this issue e.g. Cescatti (2007); Lang et al. (2010); and Pueschel et al. (2012). However, these methods have varying degrees of complexity and/or require increased levels of user input. RAW camera imagery has the advantage of increased bit-depth to aid in image classification (currently >14 bit in many commercial cameras) e.g. Jonckheere et al. (2005); Cescatti (2007); Macfarlane et al. (2014). Macfarlane et al. (2014) utilising RAW imagery in combination with automated image processing steps employing the two-corner (TC) classification method produced largely exposure insensitive results. This represents step away from traditional image processing undertaken on in-camera JPG imagery, and a step towards standardising image exposure in the field.

LR-DHP (S) displayed the poorest gap fraction agreement (Fig. 5) and subsequently highest RMSD (LAI) of all DHP and LAI-2000 method-to-method comparisons (RMSD > 0.58 LAI, Table 4). The magnitude of the plot mean LAI differences between LR-DHP (S) with HR-DHP (S) and (TC) methods was not distinctly related to site LAI (Fig. 6). Additionally, the gap fraction trend of LR-DHP (S) compared with the LAI-2200 and HR-DHP methods in Fig. 5 indicated an inconsistent detection of gap sizes with both plot and zenith angle. The HR-DHP camera has approximately 11 times the number of pixels of the LR-DHP camera. Reduced mixed pixels from finer image resolution lead to a sharper delineation of gaps and more accurate gap fraction (Blennow, 1995; Macfarlane et al., 2007a). However, the main differences observed between the HR- & LR-DHP methods may be caused by the inability to standardise LR-DHP camera exposure due to the lack of camera bracketing and image histogram preview functionality.

The effect of image resolution was unable to be rigorously tested due to poor LR-DHP image histograms, subsequently leading to the incapability of applying the automated classifications to the imagery. Additionally, the LR-DHP camera has a uniform neutral density (ND) filter with additional infra-red-cut coating, which reduces transmission by 50% at 650 ± 10 nm. The ND filter is used to uniformly reduce light intensity through the lens, usually employed in photography where a more shallow depth-of-field is desired. The ND filter introduces a need for longer exposure time to balance the reduced light transmission, thus, increasing the chance for image blur due to the handheld nature of the instrument. Utilising a camera tripod and remote trigger is recommended as means to negate increased mixed pixels from an unsteady camera.

Inherent limitations in ranging lidar instruments need to be carefully considered for estimating accurate gap fraction. The limitations stem from the potential bias induced by the interaction between the size of the lidar footprint and overlap with the intercepting target, range to target, target reflectance and orientation, and detection thresholds (Béland et al., 2014; Lovell et al., 2003; Vaccari et al., 2012). Past studies have noted that these characteristics when using a point-based gap fraction method potentially lead to a comparatively lower estimate of gap fraction, and thus, higher estimate of LAI (Danson et al., 2007; Guang et al., 2013; Lovell et al., 2003; Ramirez et al., 2013; Vaccari et al., 2012). This is due to more partial hits occurring around the edges of vegetation (Vaccari et al., 2012) and returning an intensity value above the instruments detection threshold. In addition, as the zenith angle increases, the path length of the lidar pulse through the canopy increases proportionally with lidar footprint size, thus, increasing the probability of interception and partial returns (Hancock et al., 2014). This may explain the faster rate of decrease of TLS gap fraction, lower openness, and higher LAI comparatively to HR-DHP methods (Figs. 4 and 6 and Table 4).

The closely matching gap fraction trend with zenith angle between the TLS with HR-DHP (S) and (TC) methods, combined with high R^2 for openness and LAI ($R^2 > 0.79$), indicates a poten-

tial for instrument calibration (Fig. 4, Table 4). Vaccari et al. (2012) found that a closer agreement of TLS gap fraction with DHP could be obtained using a morphology filter. Interestingly, the higher R^2 was observed for TLS with HR-DHP (TC) over (S), both for openness and LAI (0.88 and 0.79, respectively – R^2 matched for openness and LAI). Vaccari et al. (2012) found TLS produced gap fraction around 0.1–0.2 lower than DHP. In this study, TLS gap fraction was between 0 and 0.1 lower at zenith compared to HR-DHP (S) and (TC) methods, with differences increasing to around 0.1–0.2 at the 60° zenith angle. Although the same TLS instrument model and point-based gap fraction method were used in both studies, the manual DHP classification threshold and different camera exposure method employed by Vaccari et al. (2012) make a direct comparison to this study difficult. In addition, gap fraction differences as a function of zenith were not shown. Despite, systematic errors between operators not being a factor in this study due to using only one experienced operator to manually classify all images, the nature of supervised or manual classifications will always lead to some errors from subjectivity. The higher R^2 of TLS with the automated (TC) method may be explained by the avoidance of operator induced subjectivity from the manual (S) approach.

Alternatively, a number of methods for correcting partial-return bias on gap fraction estimates has been presented (Hancock et al., 2014; Jupp et al., 2009; Ramirez et al., 2013; Seidel et al., 2012). Ramirez et al. (2013) increased gap fraction estimates by around 0.35 when applying an intensity scaling method to the point-based gap fraction estimates. However, the scanner used in their study had a beam divergence of 2.7 mrad, a factor of 9 larger than the TLS used in this study (Table 2). Therefore, a greater proportion of partial returns is expected with increasing beam divergence, leading to an application of a larger correction factor. Specific measures to rectify the potential source of error for partial returns was not attempted in this study due to: (i) the ill-posed nature of intensity scaling of return data (Béland et al., 2014; Hancock et al., 2014); (ii) the recording of intensity values is instrument specific and proprietary protected information for commercial scanners requiring calibration (Kaasalainen et al., 2009); and (iii) the point-based method is an efficient and repeatable approach to estimate gap fraction (Danson et al., 2007). Intensity scaling requires further examination. These ongoing research issues are currently being investigated in activities conducted by groups such as the Terrestrial Laser Scanning International Interest Group (TLSIIG, 2014).

Further analysis of the TLS intensity imagery revealed that in RC1, the TLS returns from objects very close to the scanner (<1.5 m) were recorded as pulses with no return, i.e. it was not possible to distinguish between a gap and the absence of a measurement. This is a potential limitation of the TLS due to minimum range resolution. Finding an unobstructed area was difficult due to the complex and dense nature of the Robson Creek rainforest site. This effect was not found in any other sites. Masking pulses with missing data was not attempted due to this being subjective and thus likely to bias results.

5. Conclusion

This study compared forest canopy openness, gap fraction, and effective LAI estimates derived from common and experimental indirect ground-based instruments; all of which can be used to validate satellite-derived products of LAI, or up-scale to an intermediate high-resolution dataset. Measurements were collected and processed following standard operational protocols across five diverse forest systems in Eastern Australia. The specific instruments tested were high- and low-resolution (HR and LR), digital hemispherical photography (DHP), the LAI-2200 plant canopy analyser, and a terrestrial laser scanner (TLS).

The HR-DHP supervised (S) classification matched closely with the two-corner (TC) automated approach (RMSD 0.18 LAI) across all plots with no bias and no significant differences with openness and LAI ($p > 0.9$). These methods produced gap fraction and LAI to within ±10% (RMSD < 0.2) of the LAI-2200 in a subset of plots where the instrument was used (openness and LAI not significantly different, $p > 0.75$). Additionally, the (TC) and (S) methods produced canopy openness and LAI values within 6% of each other, across the entire range of values (openness range 0.02–0.6, LAI 0.5–5.5). However, the HR-DHP global (G) method estimated higher openness, gap fraction and lower LAI than all other methods (statistically significant differences in openness and LAI, $p < 0.05$). HR-DHP (G) produced on average 30% higher LAI than HR-DHP (S) and (TC) classifications. It was also less sensitive to within-plot LAI range as estimated by the (S) and (TC) methods. The automated (G) classification does not take advantage of first classifying homogenous regions of sky and canopy in images following the (TC) method, and is therefore, subject to larger differences than if the classification was applied to only mixed pixels. Consequently, both (TC) and (S) methods are recommended over the (G) method. In addition, the automated (TC) method can be used as a substitute for the manual (S) approach due to the comparable performance.

The LR-DHP (S) method produced a high level of variability between all methods (RMSD > 0.5 LAI). This was attributed in part to the difficulty of acquiring quality exposed images without previewing the image histogram and a greater likelihood of mixed pixels due to the low resolution and handheld nature. Both these limitations have the potential to be overcome with higher resolution cameras making use of the greater bit-depth of raw imagery and subsequent image processing leading to predominantly exposure insensitive results (Macfarlane et al., 2014).

A strong linear relationship with canopy openness and LAI metrics was found for TLS with the HR-DHP (S) and (TC) methods ($R^2 = 0.79$ and 0.88, respectively). Although TLS was on average around 55% higher for openness and LAI (significantly different, $p < 0.05$), the strong coefficient of determination indicated the potential to calibrate these methods to overcome the large offset in the reduced major axis regression. Potential TLS biases need to be quantified through further instrument calibrated efforts. Additionally, the stronger correlation was found with TLS and the automated (TC) method over the supervised (S) method, thus, indicating the potential for the (TC) method to be used as a more stable estimate than the subjective (S) classification. Temporal consistency is especially important for the validation of satellite product time-series, critical to study seasonality and vegetation phenology.

These results demonstrate variability between commonly utilised indirect ground-based methods, need to be further reduced in order to provide repeatable unbiased and accurate validation estimates, to meet product accuracy targets as low as 5%, a stated target accuracy of the WMO (2014). The discrimination between random and systematic errors caused by different ground-based methods across a range of acquisition environments merits further investigation. Computer simulation modelling may provide an appropriate means to determine each method's absolute accuracy, a task that is almost impossible to quantify in real-world forests (Hancock et al., 2014; Leblanc and Fournier, 2014; Ramirez et al., 2013). In addition, the scientific validation community would benefit from more rigorous ground-based data collection and processing protocols that would help harmonise estimates obtained from a variety of instruments.

Acknowledgements

The authors would like to acknowledge and thank various sources that provided support for this study. The funding that sup-

ported this study came from the Australian Postgraduate Award and Cooperative Research Centre for Spatial Information (CRC-SI). The CRC-SI's activities are funded in part by the Australian Government's Cooperative Research Centres Programme. Thanks to the TERN/AusCover nodes that provided access to sites, support while in the field, and data. Dr Kim Calders (WUR), Dr Darius Culvenor (Environmental Sensing Systems) and Dr Glenn Newnham (CSIRO) assisted with data provision and instrument access. Professor Mark Shortis (RMIT University) for his assistance with the Nikon D90 camera calibration. The TLSIIG Brisbane (2013), laser scanning participants collaborated with shared data and helpful discussions. Professor Bingfang Wu (RADI, CAS, Beijing) gave helpful advice and guidance. Dr Craig Macfarlane for providing the DCP processing software and instructions.

References

Anderson, M.C., 1981. The geometry of leaf distribution in some South-eastern Australian forests. Agric. Meteorol. 25, 195–206, http://dx.doi.org/10.1016/0002-1571(81)90072-8.

Ashton, D., 1976. The development of even-aged stands of *Eucalyptus regnans* F. Muell. in central Victoria. Aust. J. Bot. 24 (3), 397–414 http://dx.doi.org/10.1071/BT9760397

Baret, F., Hagolle, O., Geiger, B., Bicheron, P., Miras, B., Huc, M., Berthelot, B., Niño, F., Weiss, M., Samain, O., Roujean, J.L., Leroy, M., 2007. LAI, fAPAR and fCover CYCLOPES global products derived from VEGETATION. Part 1: principles of the algorithm. Remote Sens. Environ. 110 (3), 275–286, http://dx.doi.org/10.1016/j.rse.2007.02.018.

Baret, F., Weiss, M., Lacaze, R., Camacho, F., Makhmara, H., Pacholcyzk, P., Smets, B., 2013. GEOV1: LAI and FAPAR essential climate variables and FCOVER global time series capitalizing over existing products. Part 1: principles of development and production. Remote Sens. Environ. 137 (0), 299–309 http://dx.doi.org/10.1016/j.rse.2012.12.027

Beaudet, M., Messier, C., 2002. Variation in canopy openness and light transmission following selection cutting in northern hardwood stands: an assessment based on hemispherical photographs. Agric. For. Meteorol. 110 (3), 217–228 http://dx.doi.org/10.1016/S0168-1923(01)289-1

Beckschäfer, P., Seidel, D., Kleinn, C., Xu, J., 2013. On the exposure of hemispherical photographs in forests. J. Biogeosci. For. 6 (4), 228–237, http://dx.doi.org/10.3832/ifor0957-006.

Béland, M., Baldocchi, D.D., Widlowski, J.-L., Fournier, R.A., Verstraete, M.M., 2014. On seeing the wood from the leaves and the role of voxel size in determining leaf area distribution of forests with terrestrial LiDAR. Agric. For. Meteorol. 184 (0), 82–97 http://dx.doi.org/10.1016/j.agrformet.2013.09.005

Blennow, K., 1995. Sky view factors from high-resolution scanned fish-eye lens photographic negatives. J. Atmos. Oceanic Technol. 12 (6), 1357–1362, http://dx.doi.org/10.1175/1520-0426(1995)012<1357:SVFFHR>2.0.CO;2.

Bradford, M., Metcalfe, D., Ford, A., Liddell, M., McKeown, A., 2014. Floristics, stand structure and above ground biomass of a 25 ha rainforest plot in the Wet Tropics of Australia. J. Trop. For. Sci. 26 (4), 543–553.

Bréda, N.J.J., 2003. Ground-based measurements of leaf area index: a review of methods, instruments and current controversies. J. Exp. Bot. 54 (392), 2403–2417, http://dx.doi.org/10.1093/jxb/erg263.

Camacho, F., Cernicharo, J., Lacaze, R., Baret, F., Weiss, M., 2013. GEOV1: LAI, FAPAR essential climate variables and FCOVER global time series capitalizing over existing products. Part 2: validation and intercomparison with reference products. Remote Sens. Environ. 137, 310–329 http://dx.doi.org/10.1016/j.rse.2013.02.030

Chason, J.W., Baldocchi, D.D., Huston, M.A., 1991. A comparison of direct and indirect methods for estimating forest canopy leaf area. Agric. For. Meteorol. 57 (1–3), 107–128.

CEOS, 2014. Global LAI Product Validation Validation Good Practices v2.0. In: Fernandes, R., Plummer, S., Nightingale, J. (Eds.).

Cescatti, A., 2007. Indirect estimates of canopy gap fraction based on the linear conversion of hemispherical photographs: methodology and comparison with standard thresholding techniques. Agric. For. Meteorol. 143 (1–2), 1–12 http://dx.doi.org/10.1016/j.agrformet.2006.04.009

Chen, J.M., Black, T.A., 1991. Measuring leaf area index of plant canopies with branch architecture. Agric. For. Meteorol. 57 (1–3), 1–12.

Chen, J.M., Black, T.A., 1992. Defining leaf area index for non-flat leaves. Plant Cell Environ. 15 (4), 421–429.

Chen, J.M., Black, T.A., Adams, R.S., 1991. Evaluation of hemispherical photography for determining plant area index and geometry of a forest stand. Agric. For. Meteorol. 56 (1–2), 129–143.

Cihlar, J., Chen, J., Li, Z., 1997. On the validation of satellite-derived products for land applications. Can. J. Remote Sens. 23 (4), 381–389.

Coops, N.C., Smith, M.L., Jacobsen, K.L., Martin, M., Ollinger, S., 2004. Estimation of plant and leaf area index using three techniques in a mature native eucalypt canopy. Aust. Ecol. 29 (3), 332–341, http://dx.doi.org/10.1111/j.1442-9993.2004.01370.x.

Danson, F.M., Gaulton, R., Armitage, R.P., Disney, M., Gunawan, O., Lewis, P., Pearson, G., Ramirez, A.F., 2014. Developing a dual-wavelength full-waveform terrestrial laser scanner to characterize forest canopy structure. Agric. For. Meteorol. 198–199, 7–14 http://dx.doi.org/10.1016/j.agrformet.2014.07.007

Danson, F.M., Hetherington, D., Morsdorf, F., Koetz, B., Allgower, B., 2007. Forest canopy gap fraction from terrestrial laser scanning. Geosci. Remote Sens. Lett. IEEE 4 (1), 157–160.

De Kauwe, M.G., Disney, M.I., Quaife, T., Lewis, P., Williams, M., 2011. An assessment of the MODIS collection 5 leaf area index product for a region of mixed coniferous forest. Remote Sens. Environ. 115 (2), 767–780, http://dx.doi.org/10.1016/j.rse.2010.11.004.

Deng, F., Chen, J.M., Plummer, S., Chen, M., Pisek, J., 2006. Algorithm for global leaf area index retrieval using satellite imagery. Geosci. Remote Sens. IEEE Trans. 44 (8), 2219–2229, http://dx.doi.org/10.1109/TGRS.2006.872100.

DEWR, 2007. Australia's Native Vegetation: A summary of Australia's Major Vegetation Groups. In: A Government (Ed.). Canberra, ACT.

Fang, H., Wei, S., Liang, S., 2012. Validation of MODIS and CYCLOPES LAI products using global field measurement data. Remote Sens. Environ. 119, 43–54.

Garrigues, S., Lacaze, R., Baret, F., Morisette, J.T., Weiss, M., Nickeson, J.E., Fernandes, R., Plummer, S., Shabanov, N.V., Myneni, R.B., Knyazikhin, Y., Yang, W., 2008a. Validation and intercomparison of global Leaf Area Index products derived from remote sensing data. J. Geophys. Res. 113 (2).

Garrigues, S., Shabanov, N.V., Swanson, K., Morisette, J.T., Baret, F., Myneni, R.B., 2008b. Intercomparison and sensitivity analysis of Leaf Area Index retrievals from LAI-2000, AccuPAR, and digital hemispherical photography over croplands. Agric. For. Meteorol. 148 (8–9), 1193–1209, http://dx.doi.org/10.1016/j.agrformet.2008.02.014.

GCOS, 2011. Systematic Observation Requirements for Satellite-based Data Products for Climate. In: WM Organisation (Ed.). vol. 154. GCOS, Switzerland.

Gholz, H.L., 1982. Environmental limits on aboveground net primary production, leaf area, and biomass in vegetation zones of the Pacific Northwest. Ecology 63 (2), 469–481, http://dx.doi.org/10.2307/1938964.

Gobron, N., 1997. Theoretical limits to the estimation of the leaf area index on the basis of visible and near-infrared remote sensing data. IEEE Trans. Geosci. Remote Sens. 35 (6), 1438–1445.

Grier, C.C., Running, S.W., 1977. Leaf area of mature northwestern coniferous forests: relation to site water balance. Ecology 58 (4), 893–899.

GTOS, 2009. Assessment of the status of the development of the standards for the Terrestrial Essential Climate Variables: LAI. In: GTOS (Ed.). GTOS 66.

Guang, Z., Moskal, L.M., Soo-Hyung, K., 2013. Retrieval of effective leaf area index in heterogeneous forests with terrestrial laser scanning. Geosci. Remote Sens. IEEE Trans. 51 (2), 777–786, http://dx.doi.org/10.1109/TGRS.2012.2205003.

Hancock, S., Essery, R., Reid, T., Carle, J., Baxter, R., Rutter, N., Huntley, B., 2014. Characterising forest gap fraction with terrestrial lidar and photography: an examination of relative limitations. Agric. For. Meteorol. 189–190, 105–114 http://dx.doi.org/10.1016/j.agrformet.2014.01.012

Hero, J.M., Castley, J.G., Butler, S.A., Lollback, G.W., 2013. Biomass estimation within an Australian eucalypt forest: meso-scale spatial arrangement and the influence of sampling intensity. For. Ecol. Manage. 310 (0), 547–554 http://dx.doi.org/10.1016/j.foreco.2013.08.062

Hill, M.J., Senarath, U., Lee, A., Zeppel, M., Nightingale, J.M., Williams, R.J., McVicar, T.R., 2006. Assessment of the MODIS LAI product for Australian ecosystems. Remote Sens. Environ. 101 (4), 495–518, http://dx.doi.org/10.1016/j.rse.2006.01.010.

ICOS, 2014. Protocol Ancillary Data in Forests. In: Gielen, B., Beeck, M.O.d. (Eds.).

Jonckheere, I., Fleck, S., Nackaerts, K., Muys, B., Coppin, P., Weiss, M., Baret, F., 2004. Review of methods for in situ leaf area index determination part I. Theories, sensors and hemispherical photography. Agric. For. Meteorol. 121 (1–2), 19–35, http://dx.doi.org/10.1016/j.agrformet.2003.08.027.

Jonckheere, I., Nackaerts, K., Muys, B., Coppin, P., 2005. Assessment of automatic gap fraction estimation of forests from digital hemispherical photography. Agric. For. Meteorol. 132 (1–2), 96–114 http://dx.doi.org/10.1016/j.agrformet.2005.06.003

Jupp, D.L.B., Culvenor, D.S., Lovell, J.L., Newnham, G.J., Strahler, A.H., Woodcock, C.E., 2009. Estimating forest LAI profiles and structural parameters using a ground-based laser called 'Echidna®'. Tree Physiol. 29 (2), 171–181.

Kaasalainen, S., Krooks, A., Kukko, A., Kaartinen, H., 2009. Radiometric calibration of terrestrial laser scanners with external reference targets. Remote Sens. 1 (3), 144–158.

Knyazikhin, Y., Martonchik, J.V., Myneni, R.B., Diner, D.J., Running, S.W., 1998. Synergistic algorithm for estimating vegetation canopy leaf area index and fraction of absorbed photosynthetically active radiation from MODIS and MISR data. J. Geophys. Res. 103 (D24), 32257–32275, http://dx.doi.org/10.1029/98jd02462.

Kobayashi, H., Ryu, Y., Baldocchi, D.D., Welles, J.M., Norman, J.M., 2013. On the correct estimation of gap fraction: how to remove scattered radiation in gap fraction measurements? Agric. For. Meteorol. 174–175, 170–183 http://dx.doi.org/10.1016/j.agrformet.2013.02.013

Kucharik, C.J., Norman, J.M., Murdock, L.M., Gower, S.T., 1997. Characterizing canopy nonrandomness with a multiband vegetation imager (MVI). J. Geophys. Res.: Atmos. 102 (D24), 29455–29473, http://dx.doi.org/10.1029/97JD01175.

Lang, M., Kuusk, A., Mõttus, M., Rautiainen, M., Nilson, T., 2010. Canopy gap fraction estimation from digital hemispherical images using sky radiance models and a linear conversion method. Agric. For. Meteorol. 150 (1), 20–29 http://dx.doi.org/10.1016/j.agrformet.2009.08.001

Law, B.E., Cescatti, A., Baldocchi, D.D., 2001. Leaf area distribution and radiative transfer in open-canopy forests: implications for mass and energy exchange. Tree Physiol. 21 (12–13), 777–787, http://dx.doi.org/10.1093/treephys/21.12-13.777.
Leblanc, S.G., Chen, J.M., Fernandes, R., Deering, D.W., Conley, A., 2005. Methodology comparison for canopy structure parameters extraction from digital hemispherical photography in boreal forests. Agric. For. Meteorol. 129 (3–4), 187–207, http://dx.doi.org/10.1016/j.agrformet.2004.09.006.
Leblanc, S.G., Fournier, R.A., 2014. Hemispherical photography simulations with an architectural model to assess retrieval of leaf area index. Agric. For. Meteorol. 194 (0), 64–76 http://dx.doi.org/10.1016/j.agrformet.2014.03.016
LI-COR, 2011. LAI-2200 Plant Canopy Analyser Instruction Manual.
LI-COR, 2013. [personal communication: LAI-2200 resolution].
Lovell, J.L., Jupp, D.L.B., Culvenor, D.S., Coops, N.C., 2003. Using airborne and ground-based ranging lidar to measure canopy structure in Australian forests. Can. J. Remote Sens. 29 (5), 607–622, http://dx.doi.org/10.5589/m03-026.
Lovell, J.L., Jupp, D.L.B., Newnham, G.J., Culvenor, D.S., 2011. Measuring tree stem diameters using intensity profiles from ground-based scanning lidar from a fixed viewpoint. ISPRS J. Photogramm. Remote Sens. 66 (1), 46–55 http://dx.doi.org/10.1016/j.isprsjprs.2010.08.006
Macfarlane, C., 2011. Classification method of mixed pixels does not affect canopy metrics from digital images of forest overstorey. Agric. For. Meteorol. 151 (7), 833–840 http://dx.doi.org/10.1016/j.agrformet.2011.01.019
Macfarlane, C., Arndt, S.K., Livesley, S.J., Edgar, A.C., White, D.A., Adams, M.A., Eamus, D., 2007a. Estimation of leaf area index in eucalypt forest with vertical foliage, using cover and fullframe fisheye photography. For. Ecol. Manage. 242 (2–3), 756–763, http://dx.doi.org/10.1016/j.foreco.2007.02.021.
Macfarlane, C., Grigg, A., Evangelista, C., 2007b. Estimating forest leaf area using cover and fullframe fisheye photography: thinking inside the circle. Agric. For. Meteorol. 146 (1–2), 1–12, http://dx.doi.org/10.1016/j.agrformet.2007.05.001.
Macfarlane, C., Ryu, Y., Ogden, G.N., Sonnentag, O., 2014. Digital canopy photography: exposed and in the raw. Agric. For. Meteorol. 197, 244–253 http://dx.doi.org/10.1016/j.agrformet.2014.05.014
Mifsud, B.M., 2003. Victoria's tallest trees. Aust. For. 66 (3), 197–205, http://dx.doi.org/10.1080/00049158.2003.10674912.
Miller, J.B., 1967. A formula for average foliage density. Aust. J. Bot. 15, 141–144.
Monsi, M., Saeki, T., 1965. On the factor light in plant communities and its importance for matter production. Ann. Bot. 95 (3), 549–567, http://dx.doi.org/10.1093/aob/mci052.
Murphy, H.T., Bradford, M.G., Dalongeville, A., Ford, A.J., Metcalfe, D.J., 2013. No evidence for long-term increases in biomass and stem density in the tropical rain forests of Australia. J. Ecol. 101 (6), 1589–1597, http://dx.doi.org/10.1111/1365-2745.12163.
Pueschel, P., Buddenbaum, H., Hill, J., 2012. An efficient approach to standardizing the processing of hemispherical images for the estimation of forest structural attributes. Agric. For. Meteorol. 160 (0), 1–13 http://dx.doi.org/10.1016/j.agrformet.2012.02.007
Pueschel, P., Newnham, G., Rock, G., Udelhoven, T., Werner, W., Hill, J., 2013. The influence of scan mode and circle fitting on tree stem detection, stem diameter and volume extraction from terrestrial laser scans. ISPRS J. Photogramm. Remote Sens. 77, 44–56 http://dx.doi.org/10.1016/j.isprsjprs.2012.12.001
Ramirez, F., Armitage, R., Danson, F., 2013. Testing the application of terrestrial laser scanning to measure forest canopy gap fraction. Remote Sens. 5 (6), 3037–3056.
Rich, P.M., 1990. Characterizing plant canopies with hemispherical photographs. Remote Sens. Rev. 5 (1), 13–29.
Richardson, A.D., Dail, D.B., Hollinger, D.Y., 2011. Leaf area index uncertainty estimates for model – data fusion applications. Agric. For. Meteorol. 151 (9), 1287–1292 http://dx.doi.org/10.1016/j.agrformet.2011.05.009
Ridler, T., Calvard, S., 1978. Picture thresholding using an iterative selection method. IEEE Trans. Syst. Man Cybern. 8 (8), 630–632, http://dx.doi.org/10.1109/TSMC.1978.4310039.
Riegl, 2010. RiSCAN PRO. <http://www.riegl.com/uploads/tx_pxpriegldownloads/11_DataSheet_RiSCAN-PRO_22-09-2010_02.pdf>.
Riegl, 2013, 18/09/2013. Data Sheet. Retrieved from <http://www.riegl.com/uploads/tx_pxpriegldownloads/DataSheet_VZ-400_18-09-2013.pdf> (10.10.14.).
Ross, J., 1981. The Radiation Regime and Architecture of Plant Stands. Springer.
Running, S.W., 1984. Microclimate control of forest productivity: analysis by computer simulation of annual photosynthesis/transpiration balance in different environments. Agric. For. Meteorol. 32 (3–4), 267–288 http://dx.doi.org/10.1016/0168-1923(84)90054-6
Running, S.W., Coughlan, J.C., 1988. A general model of forest ecosystem processes for regional applications I. Hydrologic balance, canopy gas exchange and primary production processes. Ecol. Modell. 42 (2), 125–154 http://dx.doi.org/10.1016/0304-3800(88)90112-3
Ryu, Y., Nilson, T., Kobayashi, H., Sonnentag, O., Law, B.E., Baldocchi, D.D., 2010. On the correct estimation of effective leaf area index: does it reveal information on clumping effects? Agric. For. Meteorol. 150 (3), 463–472.
Schaefer, M.T., Farmer, E., Soto-Berelov, M., Woodgate, W., Jones, S., 2014. Validation of LAI and FPAR products. In: Soto-Berelov, M.A., Held Phinn, S., Jones, S. (Eds.), AusCover Good Practice Guidelines: A Technical Handbook Supporting Calibration and Validation Activities of Remotely Sensed Data Products. TERN AusCover http://data.auscover.org.au/xwiki/bin/view/Good+Practice+Handbook/WebHome
Seidel, D., Fleck, S., Leuschner, C., 2012. Analyzing forest canopies with ground-based laser scanning: a comparison with hemispherical photography. Agric. For. Meteorol. 154–155, 1–8 http://dx.doi.org/10.1016/j.agrformet.2011.10.006
Skiljan, I., 2013. IrfanView (Version 4.36). Vienna University of Technology, Vienna.
Spanner, M.A., Pierce, L.L., Peterson, D.L., Running, S.W., 1990. Remote sensing of temperate coniferous forest leaf area index. The influence of canopy closure, understory vegetation and background reflectance. Int. J. Remote Sens. 11 (1), 95–111.
TERN, 2013. Canopy – Understorey LAI Protocol Draft. In: Network, A.S. (Ed.).
TLSIIG, 2014. Terrestrial Laser Scanning International Interest Group. Retrieved from <http://128.197.168.195/?page_id=37> (21.02.14.).
Tree, D.J., Walter, G.H., 2012. Diversity and abundance of fungivorous thrips (Thysanoptera) associated with leaf-litter and bark across forest types and two tree genera in subtropical Australia. J. Nat. Hist. 46 (47–48), 2897–2918, http://dx.doi.org/10.1080/00222933.2012.737037.
Vaccari, S., van Leeuwen, M., Calders, K., Coops, N.C., Herold, M., 2012. Bias in lidar-based canopy gap fraction estimates. Remote Sens. Lett. 4 (4), 391–399, http://dx.doi.org/10.1080/2150704X.2012.742211.
Weiss, M., 2014. Pers. Comm., 15/10/2014.
Weiss, M., Baret, F., 2014. CAN-EYE V6.313 USER MANUAL: INRA.
Welles, J., 1990. Some indirect methods of estimating canopy structure. Remote Sens. Rev. 5 (1), 31–43, http://dx.doi.org/10.1080/02757259009532120.
Welles, J.M., Norman, J., 1991. Instrument for indirect measurement of canopy architecture. Agron. J. 83 (5), 818–825.
Whitford, K., Colquhoun, I., Lang, A., Harper, B., 1995. Measuring leaf area index in a sparse eucalypt forest: a comparison of estimates from direct measurement, hemispherical photography, sunlight transmittance and allometric regression. Agric. For. Meteorol. 74 (3–4), 237–249.
WMO, 2014. Requirements defined for Leaf Area Index (LAI). v 0.9.4.2. WMO, Retrieved from <http://www.wmo-sat.info/oscar/variables/view/98> (07.03.14.).
Zhang, Y., Chen, J.M., Miller, J.R., 2005. Determining digital hemispherical photograph exposure for leaf area index estimation. Agric. For. Meteorol. 133 (1–4), 166–181, http://dx.doi.org/10.1016/j.agrformet.2005.09.009.
Zhao, F., Strahler, A.H., Schaaf, C.L., Yao, T., Yang, X., Wang, Z., Schull, M.A., Román, M.O., Woodcock, C.E., Olofsson, P., Ni-Meister, W., Jupp, D.L.B., Lovell, J.L., Culvenor, D.S., Newnham, G.J., 2012. Measuring gap fraction, element clumping index and LAI in Sierra Forest stands using a full-waveform ground-based lidar. Remote Sens. Environ. 125, 73–79 http://dx.doi.org/10.1016/j.rse.2012.07.007
Zheng, G., Moskal, L.M., 2009. Retrieving leaf area index (LAI) using remote sensing: theories, methods and sensors. Sensors 9 (4), 2719–2745.